Experimental and Numerical Studies on the Premixed Syngas Swirl Flames in a Model Combustor

Nor Afzanizam Samiran[a,b], Cheng Tung Chong[c,*], Jo-Han Ng[d], , Manh-Vu Tran[e], Hwai Chyuan Ong[f], Agustin Valera-Medina[g], William Woei Fong Chong[h], Mohammad Nazri Mohd Jaafar[h]

[a] Faculty of Engineering Technology, Universiti Tun Hussein Onn Malaysia, Pagoh Higher Education Hub, 84600 Pagoh, Muar, Johor, Malaysia.
[b] Plant Reliability and Process Technology Focus Group, Universiti Tun Hussein Onn Malaysia, Pagoh Higher Education Hub, 84600 Pagoh, Muar, Johor, Malaysia.
[c] China-UK Low Carbon College, Shanghai Jiao Tong University, Lingang, Shanghai 201306, China.
[d] Faculty of Engineering and Physical Sciences, University of Southampton Malaysia (UoSM), 79200 Iskandar Puteri, Johor, Malaysia.
[e] School of Engineering, Monash University Malaysia, Jalan Lagoon Selatan, 47500 Bandar Sunway, Selangor,
[f] Department of Mechanical Engineering, Faculty of Engineering, University of Malaya, 50603 Kuala Lumpur, Malaysia.
[g] College of Physical Sciences and Engineering, Cardiff University, Wales, UK
[h] School of Mechanical Engineering, Faculty of Engineering, Universiti Teknologi Malaysia, 81310 Skudai, Johor, Malaysia

Abstract

Experimental and numerical investigations were performed to study the combustion characteristics of synthesis gas (syngas) under premixed swirling flame mode. Four different type of syngases, ranging from low to high H_2 content were tested and simulated. The global flame structures and post emission results were obtained from experimental work, providing the basis of validation for simulations using flamelet generated manifold (FGM) modelling approach via a commercial computational fluid dynamic software. The FGM method was shown to provide reasonable agreement with experimental result, in particular the post-exhaust emissions and global flame shapes. Subsequently, the FGM method was adopted to model the flame structure and predict the radical species in the reaction zones. Simulation result shows that H_2-enriched syngas has lower peak flame temperature with lesser NO species formed in the reaction zone.

Keywords: H_2-rich syngas, premixed swirl, Flamelet generated manifold, emission, flame structure, reaction zone species

1. Introduction

The need to reduce post combustion emissions is of utmost importance as pollutions inevitably endanger environment and human health. The reliance on fossil fuel over the last few decades for power generation has resulted in the production of high concentration of pollutant emissions, in particular greenhouse gases such as CO_2 and harmful pollutants such as NO_x, CO and unburned hydrocarbon. One way to reduce emissions is via the development of clean alternative fuel that can replace or substitute conventional fossil fuels. In recent years, synthesis gas (syngas) derived from biomass is considered as one of the potential alternative fuel for power generation industry [1, 2]. Syngas is a gas mixture consists primarily of H_2 and CO, which can be produced from various thermochemical processes including pyrolysis, gasification and catalytic reforming [3]. Direct application of syngas fuel in ground transportation or stationary combustion devices can potentially reduce pollutant emissions such as SO_x, NO_x, particulate matter and heavy metals [4, 5].

Syngases with high composition of H_2 have gained much attention due to the high energy content per mass and clean combustion characteristic [6]. H_2-rich syngases exhibit high flame propagation speed with wide flammability limit. The laminar flame speed of H_2 is typically eight times higher compared to natural gas, thus increasing the H_2 volume content reduces the combustion duration (the period between start of combustion and end of combustion where accumulated heat release occurs at 10% and 90 % respectively [7]), leading to the increase of combustion efficiency [8]. The high hydrogen content in syngas is also known to extend the lean operating limits of burners and exhibit the characteristics of inhibiting extinction in turbulent and strained flame environment [8-10]. However, the emissions of NO_x for hydrogen diffusion flame was shown to increase due to the high calorific value and flame temperature [11, 12]. To move

towards low emission and hydrogen economy, development of lean premixed combustion technology is emphasised, such as the dry low NO_x combustor in gas turbines and homogeneous charge compression ignition internal combustion engines [5].

Lean premixed combustion can achieve higher thermal efficiency and lower NO_x emission levels [8, 13]. This technology is widely used in land-based power generation gas turbines. The interest of using syngases in lean premixed combustor is motivated by the need to achieve emissions reduction [14, 15]. In premixed swirl combustion, the mechanism of swirl is critical to achieving high mixing rates of fuel and air as well as to stabilize the flames. High strength of swirl in combustor leads to the formation of internal recirculation zone (IRZ), which is a vortex breakdown phenomenon in fluid mechanics. The IRZ plays an important role in lean premixed by recirculating the hot products back to the flame root to assist in flame anchoring close to the burner outlet [16]. There were many fundamental experimental studies related to syngas combustion but tests under premixed swirl combustion are relatively scarce. Ge et al. [17] studied the emissions performance of non-premixed swirl syngas combustion by using a swirl burner fueled with syngases with varying H_2 content. It was reported that the amount of NO_x and CO emissions were rather constant at low H_2O dilution. Joo et al. [11] investigated H_2-rich syngas combustion with CH_4 dilution by using a partially premixed swirl burner. The NO_x and flame temperature for syngas flame were shown to reduce with the increase of CH_4 fraction. Zhang et al. [18] reported that CO_2 dilution in syngas has more profound effect on flame propagation and extinction than N_2 dilution in an opposed-jet flame under premixed condition. Alavandi et al. [19] studied the effect of CH_4 dilution on the emission of syngas combustion using a porous burner. The effect was evident, as the NOx and CO emission levels were shown to increase while maintaining the ratio of H_2:CO at 1:1. The potential use of syngas in internal combustion engine was studied by Hagos et al. [10] in a spark-ignition, direct injection engine.

Syngases diluted with CH_4 shows lower brake emissions of carbon monoxide and unburned hydrocarbon, but higher NO_X.

Apart from experimental study, numerical work on swirl premixed combustion of syngas has also been studied previously. Li et al. [20] investigated the dilution effects of CO_2 and H_2O on partially premixed swirling syngas flames with large eddy simulation (LES) method. The study employed the linear-eddy model (LEM) to resolve the chemical reaction processes using specific length and time scales for H_2-based fuel combustion. The study reported that CO_2 is more effective compared to H_2O in reducing the flame temperature. De et al. [16] investigated the effect of swirl, premixedness and geometry for hydrogen-enriched premixed flame using LES with a Thickened Flame (TF) model. The study reported that the flame dynamic in upstream region typically exhibits higher swirl strength regardless of the premixedness level and burner geometry. It was also found that premixed system is more stable under low swirl operation. Ilbas et al. [21] performed a simulation study of combustion characteristics of low calorific value syngas to investigate the effect of turbulator angle in a burner. The simulation work utilised the PDF/ Mixture Fraction and k-ε standard for combustion and turbulence model respectively. The study revealed that changes in turbulator angle affect the temperature, emission and velocity gradient. The upstream burner also exhibited high temperature zone as the turbulator angle is increased.

Simulation of syngas flame in the combustor environment is useful to probe the reactions and species involved during reactions. There are various models that can be used to simulate combustion chemistry. Tabulated chemistry method such as the Flamelet generated manifold (FGM) is used to reduce the combustion chemistry in simulation study which enables the prediction of intermediate species as well as pollutants [22]. The FGM method considers a multidimensional flame as an ensemble of one dimensional flames similar to a flamelet approach [23]. The modelling of reacting flow using FGM method has been conducted by several groups.

Verhoeven et al. [24] modelled laminar flame of methane in a co-flow of air using FGM approach and compared with full chemical model. The study shows that when Lewis number of unity is considered, the FGM method which consists of counterflow diffusion flamelets is able to predict temperature and species concentrations in good agreement with the detailed solution (with a maximum difference ~2%). Nakod et al. [23] conducted a systematic comparative study of the FGM model and laminar flamelet method (LFM) for various diffusion/premixed flames. The simulation results predicted by FGM model are more physical and accurate compared to the LFM method for all the flames tested. The numerical simulation of premixed swirl syngas flame using FGM method is relatively scarce. Hence, the present study investigates the syngas swirl flame using FGM method and compared with experimental data. Syngases of various H_2/CO composition are simulated to investigate the flame structure and emissions, followed by the examination of the detailed species distribution in the flame reaction zones.

2. Experimental

2.1 Swirl burner design and setup

The schematic diagram of a premixed swirl-stabilised flame burner is shown in Figure 1a. The fuel and air were supplied to the plenum for premixing before exiting to the burner through the swirler for ignition. The exit plane of the burner is referenced as $h = 0$ mm. The inner and outer diameters of the swirler hub are 26 mm and 40 mm respectively. The axial swirler consists of 6 straight vanes with thickness of 1.5 mm and positioned at an angle of 45^o from axial centreline axis, forming a geometrical swirl number of approximately $S_N \sim 0.84$. Swirl flow enables a central recirculation zone generated downstream of the exit plane, allowing the mixing of hot combustion products with unburned mixtures for continuous flame stabilization [25]. A quartz tube is mounted at the flange of exit plane to allow visualisation of flames. The

flow delivery system is shown in Figure 1b. The dry air was supplied and regulated via a mass flow controller (Sierra) with an accuracy of ±1.5% full scale. The gaseous fuel was supplied by mixing H_2, CO, CH_4 and CO_2 in the mixing chamber to model the syngas composition. The H_2 and CO were regulated by mass flow controllers, while CH_4 and CO_2 were regulated by mass flow controllers (Sierra, ±1.5% full scale accuracy). The mixture of air and fuel was ignited with an ignitor torch at the burner exit to establish a continuous swirl flame.

2.2 Test procedures and operating conditions

Measurements of the post combustion products including NO, CO, O_2 and CO_2 were performed at 400 mm downstream of the burner outlet using a gas analyser (Tempest 100). The gas analyser is capable of measuring NO, CO, O_2 and CO_2 in the range of 0-1000 ppm, 0-10,000 ppm, 0-25% and 0-99.9%, respectively. The emitted gas samples were induced by a suction pump in the gas analyser through a sampling probe. The sampling probe is placed 10 mm inside from the exit plane of the combustor. The emission readings were taken at 8 spatial locations radially across the burner outlet. The mean average of all the emission point was calculated using the area weighted average velocity method [26].

Table 1: Syngas composition and lower heating values at stoichiometric (ϕ = 1.0)

Syngas	Air	H_2		CO		CH_4		CO_2		LHV
	L/min	(vol%)	(L/min)	(vol%)	(L/min)	(vol%)	(L/min)	(vol%)	(L/min)	(MJ/kg)
SG1	100	67.5	23.5	22.5	7.9	5	1.7	5	1.7	25
SG2	100	49.5	17.2	40.5	14.2	5	1.7	5	1.7	17.9
SG3	100	40.5	14.0	49.5	17.3	5	1.7	5	1.7	15.7
SG4	100	22.5	7.8	67.5	23.6	5	1.7	5	1.7	12.8

Composition of the syngases used in this experiment is shown in Table 1. The test cases are designated alphanumerically as SG1-SG4, representing a range of high to low H_2-based syngases established at ϕ = 1.0. Methane and carbon dioxides are typical diluents that exist in

syngases produced from gasification of coal and biomass in minor quantity and hence are supplied at a constant 5% by volume for both gases [27, 28]. The air flow rate was set at 2 g/s for all test cases and fuel flow rates were regulated at the range of 0.1 to 0.7 g/s to form air-fuel mixtures with equivalence ratios of 0.5 to 1.0 for emission measurements. The experimental result obtained serves as target validation for simulation in the subsequent sections.

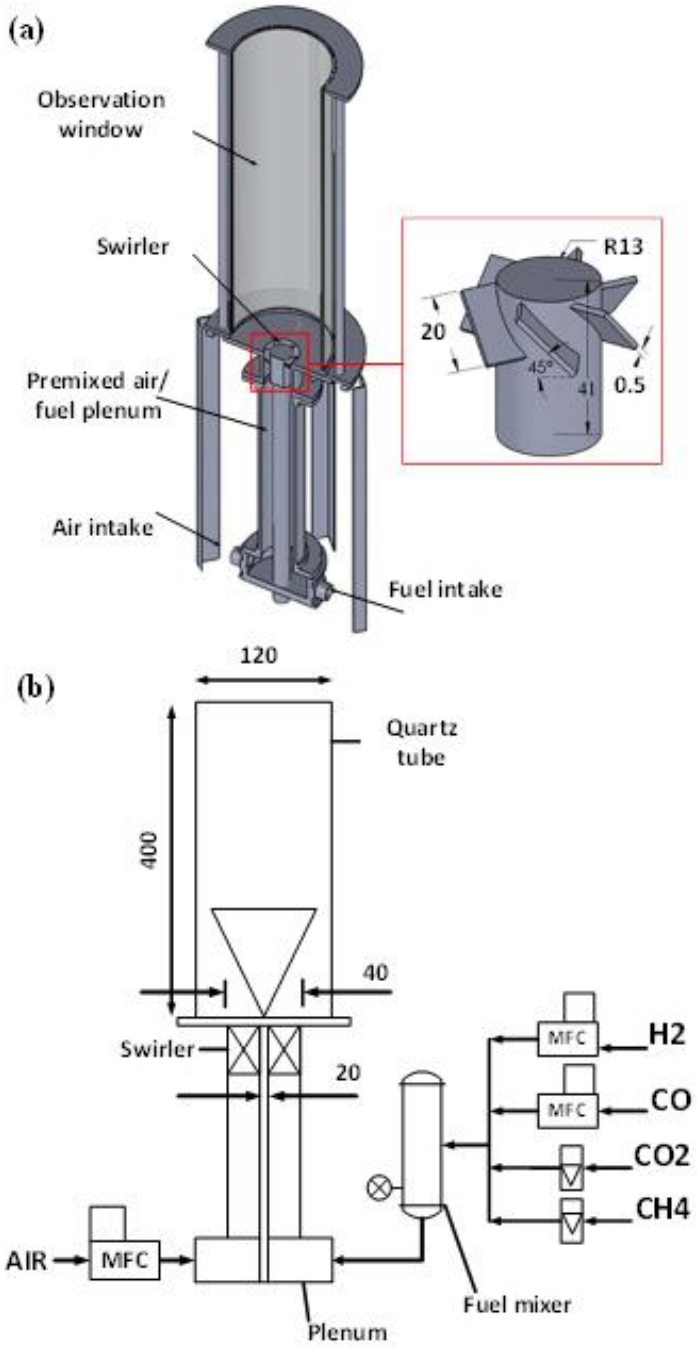

Figure 1: (a) Gaseous swirl flame burner and (b) schematic of the burner and flow delivery system

3. Numerical modelling

3.1 Flamelet generated manifold (FGM)

The flamelet in FGM method is computed with the detailed chemistry reaction scheme of GRI-Mech 3.0, of which the 325 elementary reactions and 53 species are sufficient to compute the syngas (CO, H_2, CO_2 and CH_4) combustion as well as the formation of pollutants. The FGM method directly uses the chemistry from a laminar flamelet database generated from multiple 1D flamelet calculations executed with detailed chemical kinetics and transport equations. Each flamelet contains slightly different boundary condition and the type of flamelet (either premixed or non-premixed) is determined. The premixed swirl flame in this study is modeled using the commercial CFD software *Ansys Fluent*. This study utilises the partially premixed model to simulate the premixed swirl flame in a swirl combustor.

Partially premixed combustion parameters focus on two variables that describe the reaction progress (reaction progress variable c) and mixing (mixture fraction, f). One dimensional premixed flamelet is generated to solve the flamelets in reaction progress space. The reaction progress variable is defined by the following equation:

$$c = \frac{[\sum_k \alpha_k (Y_k - Y_k^u)]}{[\sum_k \alpha_k (Y_k^{eq} - Y_k^u)]} = \frac{Y_c}{Y_c^{eq}} \quad (1)$$

Progress variable is defined as a normalised sum of the product species mass fraction over all species in the chemical mechanism. From the equation (1), Y_k denotes the k^{th} species mass fraction, superscript u denotes the unburnt reactant at the flame inlet, and superscript eq denotes chemical equilibrium at the flame outlet. The coefficient α_k is prescribed accordingly so

that the reaction progress c, increases monotonically through the flame, $\alpha_k = 0$ for all species except $\alpha_{CO_2} = \alpha_{CO} = 1$ for hydrocarbon combustion and $\alpha_{H_2O} = 1$ for fuel without C element such as H_2. The one-dimensional adiabatic flamelet equations can be transformed from physical-space to reaction-progress space.

$$\rho\frac{\partial Y_k}{\partial t}+\rho\frac{\partial Y_k}{\partial c}\dot{\omega}_c=\rho\chi_c\frac{\partial^2 Y_k}{\partial c^2}+\dot{\omega}_k \tag{2}$$

$$\rho\frac{\partial T}{\partial t}+\rho\frac{\partial T}{\partial c}\dot{\omega}_c=\rho\chi_c\frac{\partial^2 T}{\partial c^2}-\frac{1}{c_p}\sum_k h_k\dot{\omega}_k+\frac{\rho\chi_c}{c_p}\left(\frac{\partial c_p}{\partial c}+\sum_k c_{p,k}\frac{\partial Y_k}{\partial c}\right)\frac{\partial T}{\partial c} \tag{3}$$

where Y_k is the k^{th} species mass fraction, T is the temperature, ρ is the fluid density, t is time, $\dot{\omega}_k$ is the k^{th} species mass fraction rate, h is the total enthalpy and $c_{p,k}$ is the k^{th} species specific heat at a constant pressure. The scalar dissipation rate χ_c is defined as

$$X_c=\frac{\lambda}{\rho c_p}|\nabla c|^2 \tag{4}$$

where λ is the thermal conductivity. The scalar dissipation χ_c varies with c and is an input to the equation set. Equation 4 becomes

$$\rho\frac{\partial Y_k}{\partial t}+\rho\frac{\partial Y_k}{\partial c}\dot{\omega}_c=\frac{\lambda}{c_p}|\nabla c|^2\frac{\partial^2 Y_k}{\partial c^2}+\dot{\omega}_k \tag{5}$$

Apart from progress variable, mixture fraction in FGM directly corresponds to the single equivalence ratio of 1D premixed flamelet. Premixed flamelet at different mixture fractions has different maximum scalar dissipations, χ_{max}. The scalar dissipation $\chi_c(f,c)$ at any mixture fraction, f is modelled as

$$\chi_c(f,c)=\chi_{max}^{STO}\exp\left(-2\left(\text{er fc}^{-1}\left(\frac{f}{f_{STO}}\right)\right)^2\right)\exp\left(-2\left(\text{er fc}^{-1}(2c)\right)^2\right) \quad (6)$$

where STO indicates stoichiometric mixture fraction and $er\,fc^{-1}$ is the inverse complimentary error function. The scalar dissipation at stoichiometric mixture fraction, X_{max}^{sto} is hence the only model input to the premixed flamelet generator in ANSYS Fluent. The solution of unstrained (freely propagating) physical space flamelets for rich, lean and stoichiometric for hydrocarbon and H_2 flame generally match the default value of $X_{max}^{sto} = 1000/s$ at standard temperature and pressure [29].

3.2 Setup and procedure

3.2.1 Grid setup

The numerical grid is important in combustion simulation to achieve accurate result. High quality elements with low growth rate is required to simulate the burner region where high temperature and species concentration are involved. Cut shell method which primarily consists of structured hexahedron grid was chosen in this simulation study as shown in Figure 2. The grid has the size of minimum and maximum cells of 0.7 and 1 million, respectively. The mesh quality was determined by the aspect ratio and orthogonal quality. According to Zerrin et al. [30], hexahedron grid is considered to present a good quality of mesh with maximum aspect ratio of 35 and a minimum orthogonal quality of 0.15. In this case, the maximum aspect ratio was recorded at 13.43 and minimum orthogonal quality at 0.19 where both are within the range as suggested by Zerrin et al. Higher grid density of cells was constructed near the burner outlet region and became coarser when approaching the burner exit. The fine mesh corresponds to high velocity, species and temperature gradient at the burner exit.

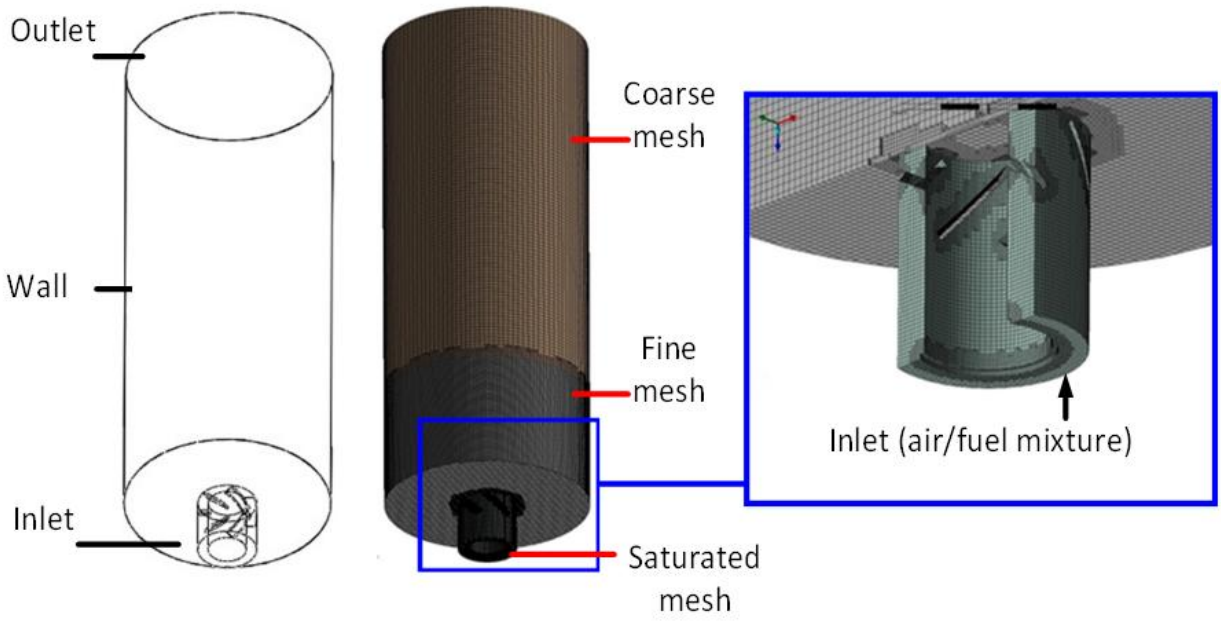

Figure 2: Boundary condition and structured hexahedron mesh

3.2.2 Boundary conditions

Syngases with various concentration of H_2 were used as operating fuels in this simulation as shown in Table 1. At the inlet, mass flow rate model setup was implemented according to the equivalence ratio. The simulations were carried out for different fuel concentration which correspond to air-fuel equivalence ratios of 0.6, 0.8 and 1, covering fuel lean and stoichiometric regions. The inlet turbulent intensity and hydraulic diameter for fuel were set to 5% and 10 mm respectively. The value of turbulent intensity is based on the value as suggested in [31]. The combustor wall was set to no-slip boundary and no-species flux condition. Flow outlet at burner exit was treated as burner outlet condition. The value of static pressure at the outlet boundary was set to zero relative to the surrounding of atmospheric pressure. Table 2 shows the detail setup of boundary conditions in computational domain.

Table 2: Applied boundary condition in CFD

	Air inlet	Fuel inlet	Outlet
Boundary type	Mass flow inlet	Mass flow inlet	Pressure outlet
Mass Flow specification method			
Mass flowrate (g/s) / gauge pressure (pascal)	2	0.1 – 0.7	0
Turbulence specification method			
Turbulent Intensity (%)	17	5	5
Hydraulic diameter (m)	0.02	0.01	0.14

3.2.3 Convergence criteria

The convergence of solution was determined by several criteria as reported by previous researchers. Mayr et al. [32, 33] stated that simulation is considered as converge if the fluctuation of maximum temperature and species concentration do not exceed 5 K and 0.001 mol fraction respectively at different points inside the combustor. The residuals for mixture fraction variance and mean mixture fraction should be less than 10^{-6} while other equations such as continuity, velocity and k-epsilon are kept below 10^{-3} [33].

Apart from residual, the number of iteration is also indicative of the convergence of simulation process. As shown in Figure 3, the changes of NO_x emission for syngas combustion for all test cases were observed to be constant at the number of iteration of approximately over 8000. As the fluctuation of NO_x value is minimal and reaches constant state, the mean value of NO_x is considered to be converged.

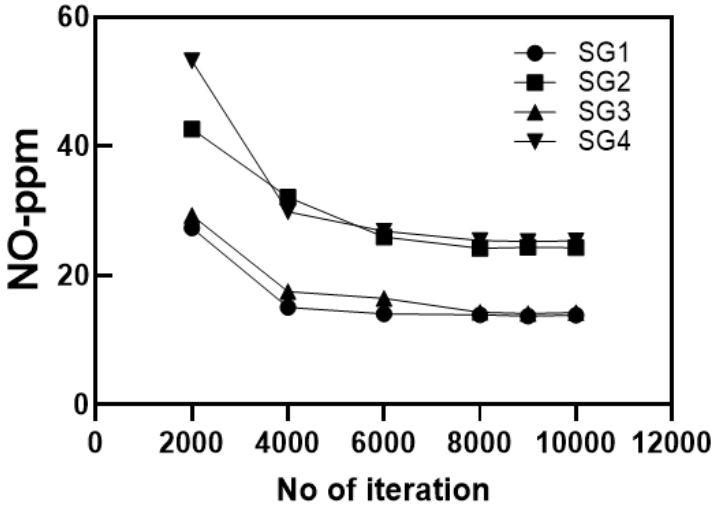

Figure 3: Solution of NO_x against the number of iteration

The grid independence study is performed using different size of mesh. The solution is considered to be grid independent when no changes occur with further refinement in the number of mesh elements or grid size. Figure 4 shows the emission of O_2 as a function of equivalence ratio for moderate H_2-rich syngas case using different size and number of cell elements for mesh. The combustion model of FGM was used for this particular investigation. The numerical and experimental results were observed to agree quite well for highest number of grid which is 1,000,000 mesh in this case. This confirms that higher accuracy result was achieved using dense mesh, despite the significant difference between different mesh numbers tested. The grid number of 800,000 was considered to have reached a point of grid independent as the result was almost identical with the case of 1,000,000 mesh.

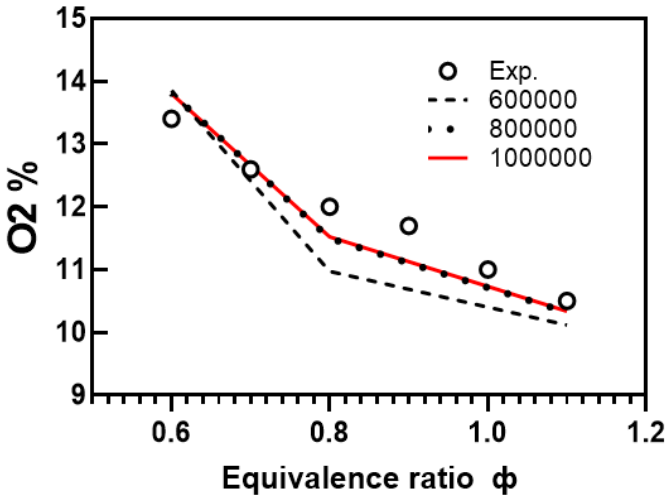

Figure 4: Emission of O_2 as a function of grid or mesh element size

3.2.4 Fluid flow modelling

In this study, the ANSYS Fluent with finite volume code was employed to solve the mass, momentum, energy and heat transfer equations. A pressure-based solver was used for steady state condition. The fluid flow is described by solving the RANS (Reynold-averaged Navier Stokes) equations. Turbulence models was used to close the RANS equations. There are a few turbulence models available in the CFD code. The standard k-ε model was utilised for the turbulence model in this simulation. A SIMPLE algorithm scheme was used to compute the pressure velocity coupling [33]. Governing equation is discretised using second order upwind scheme for the equations of momentum, turbulent kinetic energy and dissipation rate, progress variable and mixture fraction. PRESTO! scheme is applied for pressure. Mayr et al. [32] reported that PRESTO! scheme enables faster convergence in simulation.

4. Result and discussion

4.1 Exhaust gas analysis

Comparison of the predicted NO concentration from exhaust gas emissions for FGM models at different equivalence ratios against measured experimental data is shown in Figure 5. The percentage error of FGM model is also presented in Figure 5 to indicate the accuracy of the combustion model with experimental data. It is observed that FGM predictions on the concentration of NO show similar trend for all types of syngases. Prediction by FGM method showed good agreement with experimental result at lean region, especially at equivalence ratio of 0.8 and below. However, the concentration of NO_x was substantially over predicted when approaching stoichiometric region, particularly for high to moderate H_2-rich syngases (SG1 and SG2). Verhoeven *et al.* [24] suggested that premixed FGM model is less accurate compared to non-premixed FGM model. The deviations for premixed FGM is mainly caused by the fact that the species in premixed FGM could not diffuse in the direction of the gradient of Z (from reaction zone to the combustor chamber outlet). Thus, the absence of the diffusion effect in premixed FGM model is one of the factors that leads to the deviation in the concentration of NO_x.

Apart from the type of combustion, a parameter called the progress variable in FGM method is observed to be another crucial factor that causes the NO_x deviation to occur at stoichiometric condition. The progress variable is a controlling variable in FGM method which is used to parameterise the flamelet solution [34, 35]. Thus, progress variables have been conventionally defined as using the mass fraction of major species such as CO_2, CO, H_2 and H_2O with the following expression:

$$c = \frac{\frac{Y_{CO_2}}{M_{CO_2}} + \frac{Y_{H_2O}}{M_{H_2O}} + \frac{Y_{H_2}}{M_{H_2}}}{\frac{Y^{eq}_{CO_2}}{M_{CO_2}} + \frac{Y^{eq}_{H_2O}}{M_{H_2O}} + \frac{Y^{eq}_{H_2}}{M_{H_2}}} \qquad (7)$$

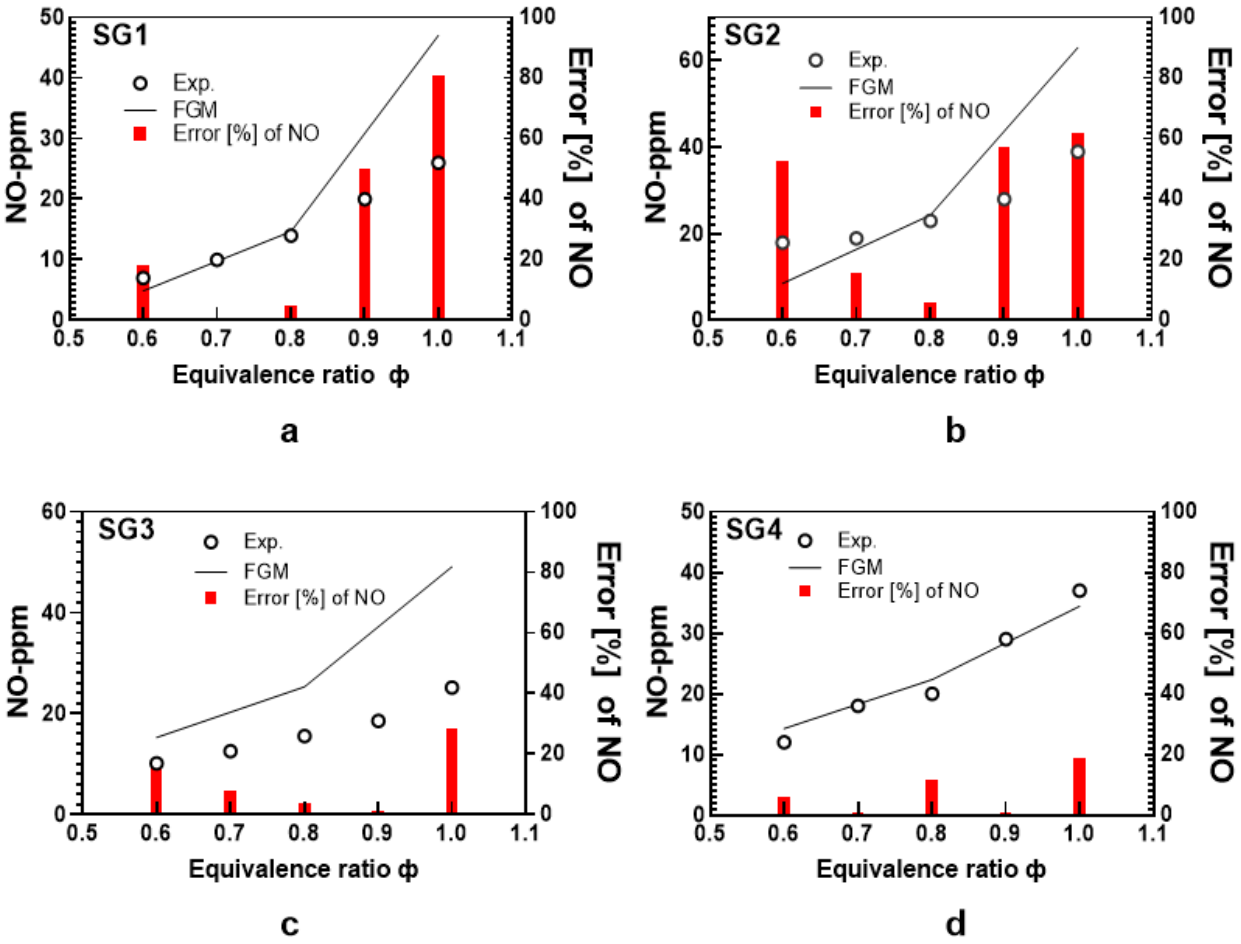

Figure 5: NO emissions for cases of (a) SG1 (b) SG2 (c) SG3 and (d) SG4 obtained from experiments and numerical simulations using FGM method as a function of equivalence ratio.

The equation of progress variable does not involve NO_x species. Van Oijen *et al.* [36] defined the NO_x species in FGM method via two approaches. The first is to include NO_x in the definition of reaction progress variable. The second is to solve the transport equation for NO_x with the source term from the look-up table. The study reported that the first approach resulted in a smoother mapping of NO_x mass fraction and its chemical source term and reduces the interpolation error. Ansys Fluent utilises the second approach to define NO_x in the FGM model. Boucher et al. [37] extracted NO reaction rate from the manifold at the given equivalence ratio based on the second approach from Van Oijen's model at the maximum value of the progress variable. This implies a linear evolution of progress variable for mass fraction of NO_x as the reaction rate is independent of the calculated NO_x concentration. This linear evolution of NO_x

equilibrates at maximum level when approaching stoichiometric or rich mixture rather than depending on the actual calculated value that it supposed to produce at that particular region. Therefore, this behaviour causes the mass fraction of NO_x to over predict when approaching stoichiometric region. Boucher et al. suggested a relaxation term to be introduced to stop the evolution of NO_x at the maximum level. The extended manifold is required to serve this purpose in which NO_x mass fraction is accounted for in the progress variable definition as proposed by van Oijen's first approach. It is recommended to use this method in future work to improve accuracy, particularly when predicting stoichiometric or rich mixture.

Surprisingly, FGM prediction shows better agreement with experimental results for very low H_2-rich (case SG4) in which the concentration of CO was higher for this particular syngas when approaching stoichiometric region. The lower flame speed and other kinetic mechanism effect of CO species in syngas was observed as one of the reasons that caused the evolution of NO_x of progress variable to slow down before reaching a maximum level. Therefore, over prediction at rich region could be avoided when simulating high CO-rich syngas.

Deviation of CO_2 species predicted by FGM model are typically below 40% error for SG1 and SG2 (H_2-rich syngas) as compared to actual experimental value as shown in Figure 6a-d. However, FGM method overpredicts the CO_2 emissions as the percentage of error increases to above 40% (Figure 6) for SG3 and SG4 cases (CO-rich syngases). Thus, the error percentage is correspondingly high as the amount of CO in syngas increases. As the progress variable in FGM model is conventionally defined as using the mass fraction of major species such as CO_2, CO and H_2O, Najafi-Yazdi et al. [38] reported that the progress variable usually yields inaccurate results for rich mixtures or heavy hydrocarbon fuels because the mass fraction is decomposed before significant heat release. High amount of CO in SG3 (low) and SG4 (very low) H_2-rich syngases along with fast decomposition effect causes the production of CO_2 species to increase in FGM model. Figure 7 shows that O_2 species is well predicted by FGM method as the error

percentage is below 20% for all syngas type. FGM method principally uses quasi-steady state approximation for fast chemical processes and this approach is well suited to predict free radical species such as O_2 [36].

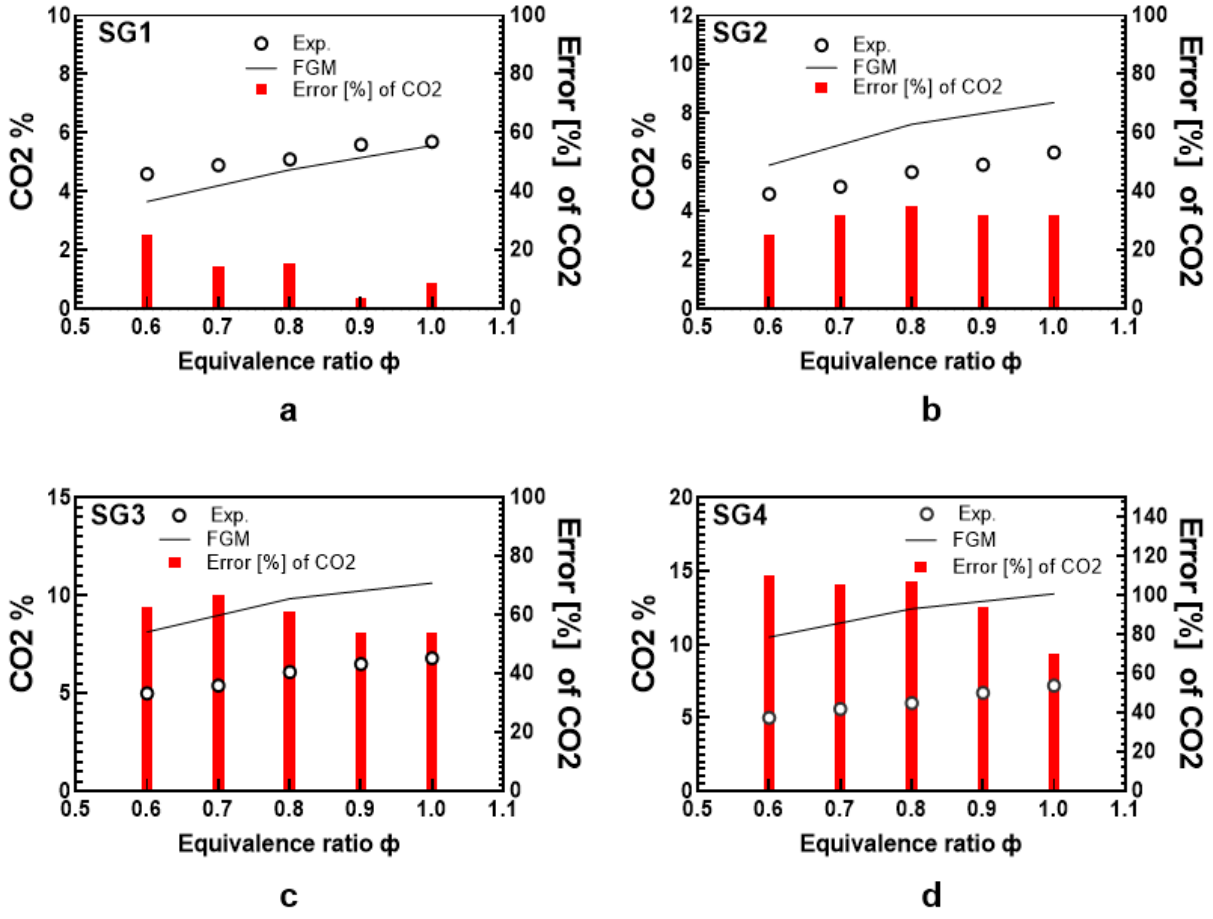

Figure 6: CO_2 emissions for case (a) SG1 (b) SG2 (c) SG3 and (d) SG4 syngases for experimental and numerical simulation using FGM method as a function of equivalence ratio.

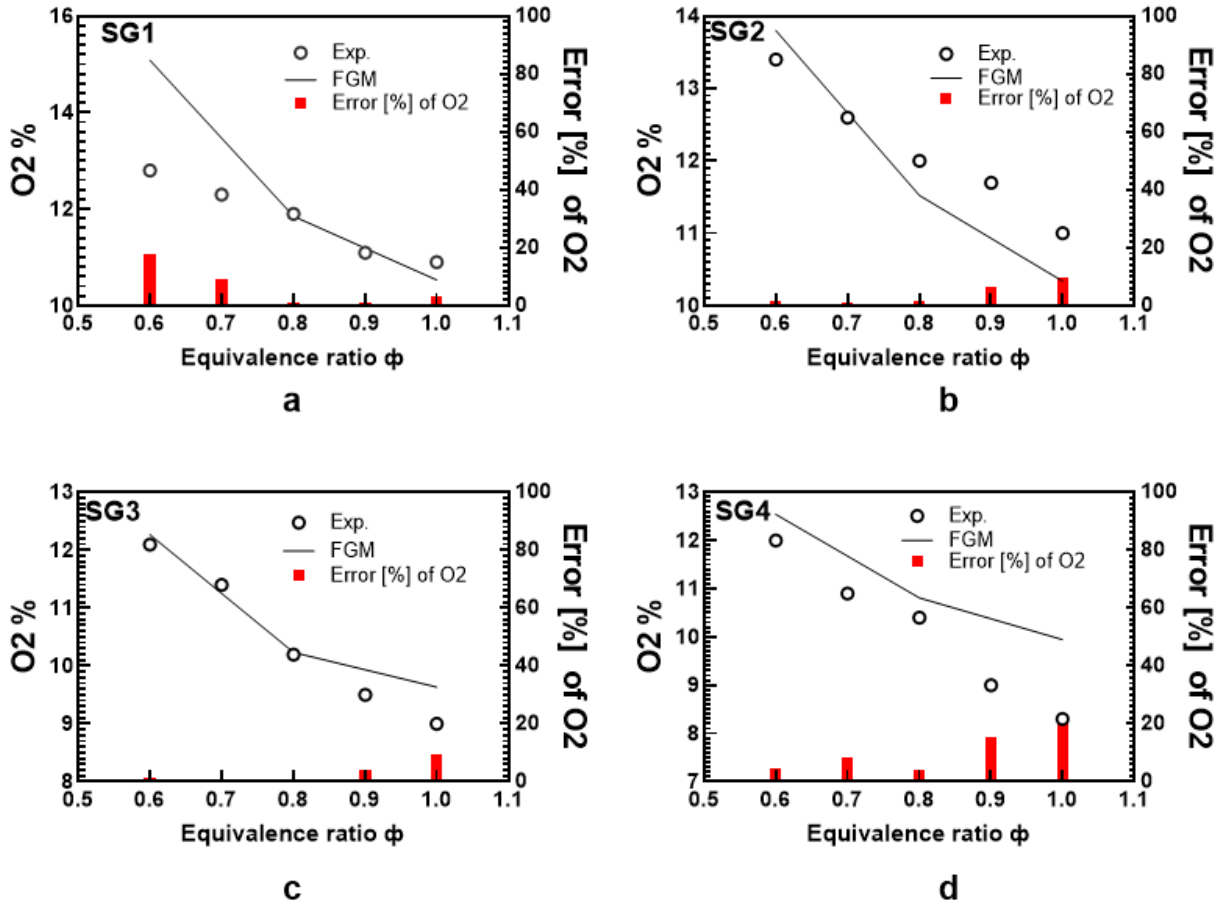

Figure 7: O_2 emissions for case (a) SG1 (b) SG2 (c) SG3 and (d) SG4 syngases for experimental and numerical simulation using FGM method as a function of equivalence ratio.

4.2 Reaction zone modelling using FGM approach

Investigation of the flame structure in terms of species mole fraction profiles in the premixed reaction zone allows more fundamental analysis on radical species such as OH, O and H. Previous sections validate the computational method with experimental result to examine the prediction accuracy. The FGM simulation result partially agree with experimental data, where the trends of the emissions of NO, CO_2 and O_2 are sufficiently simulated at the same order of magnitude. Thus, the FGM is used to extent the study on flame structure, radical species and NO prediction in the reaction zone to gain insight of the chemistry that occurs within the combustor.

4.2.1 Swirl flame structure

Study of flame height is important to investigate the shape and structure of the flame. According to Singh et al. [39], the flame height is defined by the boundary of reaction zone which appears as visible bluish flame (high temperature flame).The flame height is typically measured from the exit plane of burner (flame base) to the flame tip as illustrated in Figure 8 [39, 40]. However, this measurement is difficult to conduct in actual experimental condition. CFD simulation allows the estimation of flame height by plotting the selected value of temperature distribution. Khaleghi et al. [41] explained that the flame height in CFD analysis is measured by the distance between the fuel inlet port to the point where the flame temperature is at maximum. Figure 9 shows the temperature distribution in the vertical cross-sectional planes within the reaction zone area for all syngas types simulated using FGM method. The temperature contours are visually compared with the swirl flame appearance established experimentally at stoichiometric condition. Comparison of the images shows that simulated flames are somewhat close to the actual flame fronts. The orange and yellow contours in the simulated flames at

stoichiometric condition shows the temperature of reaction zone is above 1700 K at this condition, concurring with the location where heat release occurs in the actual flames. Figure 10 illustrates the distribution of maximum temperature across the radial distance from burner centreline for stoichiometric syngas/air mixture. The highest temperature is observed to be at the radial distance of 10 mm for SG1, while the distances for SG2, SG3 and SG4 are within 20 – 30 mm. The aforementioned radial distance is indicative of the maximum flame height location relative to the maximum flame temperature. The relation of flame height with maximum temperature is illustrated in Figure 10b.

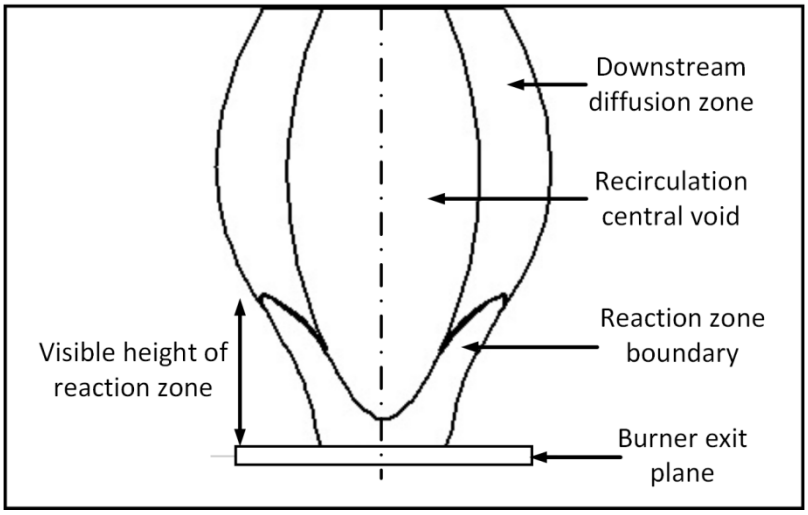

Figure 8: Different zones of swirling flame [39]

Figure 10a shows the case SG1 (high H_2-rich syngas) exhibits the lowest peak temperature owing to low CO component. The adiabatic flame temperature of CO is known to be higher than H_2 [42], thus the high temperature flame region for SG2, SG3 and SG4 (due to high adiabatic temperature of CO) extends radially outward to r/D = 0.4, owing to the extended flame front as compared to SG1. Figure 10a further shows the area under the temperature curve increases with increasing H_2 concentration. The temperature region increases as the strength of recirculation zone diminishes, hence the flame is stabilised at the surface of the burner exit. This

condition is consistent with the characteristic of local heat flux effects as reported by Veetil et al. [43]. The local heat flux value increases with the increase in percentage of hydrogen in the reacting mixture due to the high reactivity and diffusive nature of hydrogen, which assists in stabilising the flame near the surface of the burner exit [43].

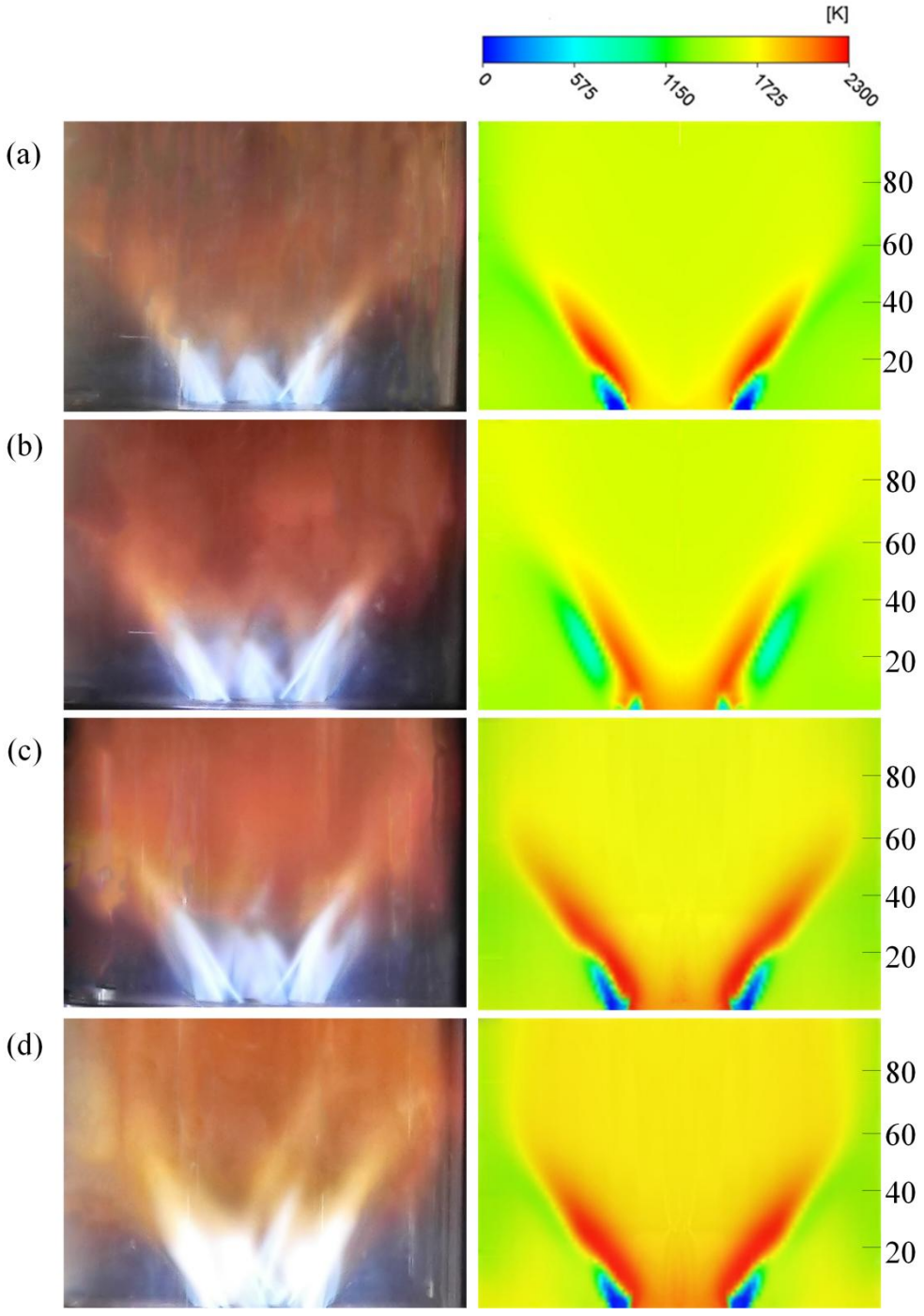

Figure 9: Flame images from experimental (left) and numerical temperature distribution (right) for (a) SG1 (high H_2) (b) SG2 (moderate H_2) (c) SG3 (low H_2) (d) SG4 (very low H_2) syngas at sthoichiometric ($\phi = 1.0$) condition.

Figure 10b depicts that SG1 syngas shows lower flame height as compared to other syngases. The lower flame height corresponds to the lower maximum temperature. High H_2 content in SG1 is one of the critical factors that results in lower flame height. In general, flame height increases with the reduction of H_2 component in syngas, which is consistent with the result as shown in previous work [11, 14]. High flame speed characteristic of H_2 component results in high reactivity at the upstream region. As the concentration of H_2 reduces, the flame propagating speed also reduces, extending the flame front towards downstream of the burner exit [44].

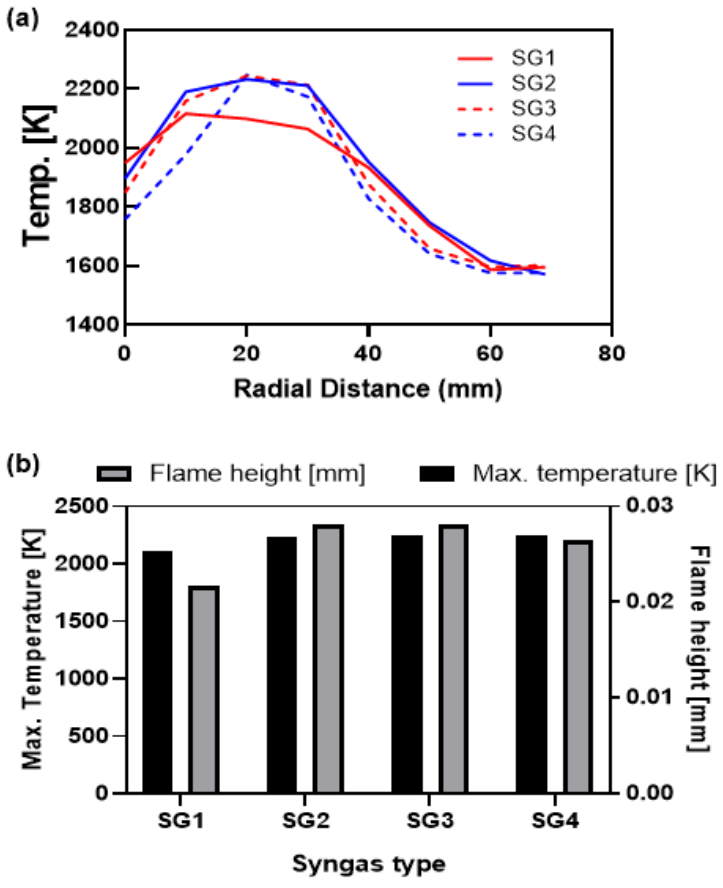

Figure 10: (a) Maximum flame temperature at different radial distance from centreline and (b) flame height for different types of syngas

4.2.2 Analysis of NO_x prediction and radical component

Comparison of the species mole fraction for NO, NO_2, OH, O and H components along the radial directions at four axial distances (z= 20, 40, 60 and 80 mm) for different composition of syngases established at $\phi = 1.0$ is shown in Figure 11 and 12. High H_2-rich syngas (SG1) is observed to produce lower NO and NO_2 compared to other syngas composition at all axial locations except at z = 40 mm, while SG2 and SG3 typically produce high concentration of NO and NO_2 at all axial locations except z = 20 mm. SG4 syngas at z = 20 mm exhibits peak NO concentration but lower value at regions close to the hub of burner mouth compared to other syngas compositions. All the NO and NO_2 values emitted by each syngas type is strongly related to the thermal NO element. The formation of thermal NO is determined by a set of highly temperature-dependent chemical reactions known as the extended Zeldovich mechanism [45]. Therefore, NO value increases with the increase of flame temperature and vice versa. Figure 11 clearly shows that SG1 emits lower NO species especially at z = 60 mm and 80 mm as the temperature at the same location is also lower compared to SG2, SG3 and SG4.

Other than temperature, the formation of thermal NO involves the radical species of O and OH as shown in the reactions below:

$$O+N_2 \leftrightarrow NO+N \quad (8)$$

$$N+O_2 \leftrightarrow NO+O \quad (9)$$

$$N+OH \leftrightarrow NO+H \quad (10)$$

The first reaction is relatively slow at low temperature and thus limits the accessibility of nitrogen (N) atoms for the other two reactions. High temperature which is greater than 1800K is needed to break the strong triple bond of nitrogen (dissociation energy of 941 kJ/mol). However, the activation energy for oxidation of N atoms in Eq.8 is low [29]. When there is appropriate

amount of oxygen, the rate of consumption of free nitrogen atoms becomes equal to the rate of its formation. The NO formation rate is therefore quantified as follows:

$$\frac{d[NO]}{dt}=2k_{f,1}[O][N_2]\frac{\left(1-\frac{k_{r,1}k_{r,2}[NO]^2}{k_{f,1}[N_2]k_{f,2}[O_2]}\right)}{\left(1-\frac{k_{r,1}[NO]}{k_{f,1}[O_2]k_{f,3}[OH]}\right)}\left[\frac{mol}{m^3 s}\right] \quad (11)$$

From this equation, oxygen (O) atoms and OH are predominantly crucial for the formation of NO [46]. Since z = 40 to 80 mm consist of temperature below 1800 K, the formation of NO is therefore highly dependent on the radical species of O and OH. In general, the trend monotonically decreases from SG2 to SG4 for OH and O species except for SG1 in which the value is typically lower than SG2. High H_2 concentration in syngas is observed to produce more OH species. This result is consistent with the data reported by Park et al. [47]. However, the high content of OH and O species in SG1 at z = 20mm does not contribute to the high production of NO species since thermal effect is more pronounced at this stage as temperature level reaches above 1800 K. High NO species for both moderate (SG2) and low (SG3) H_2-rich syngas show high concentration of O atoms at z=40 mm and 60 mm. The abundance of NO species for SG1 (high H_2-rich) at Z=40 mm indicates the availability of O species at the same axial location. SG2 (moderate H_2-rich) is observed to produce high NO but low concentration of O species at z=80 mm. This is due to the high concentration of OH species which replaces the role of O species to form NO. However, the high concentration of OH produced by SG1 (high H_2-rich) at the same level has no effect as the NO species is minimum compared to other syngas. In this case, the dual-effect of low O species and limited N atoms results in low NO formation.

The species of H radical is crucial intermediate species for NNH mechanism as indicated by the reaction NNH+O↔NO+NH and N_2+H+M↔NNH+M which promotes NO formation via

NNH path [48]. According to Xie et al. [49], NO production is primarily contributed by thermal mechanism at high temperature and low stretch rate which appears in both combustion and post flame zone. NO production by NNH mechanism is proportional to the H and O concentrations as the mechanism is relatively insensitive to temperature and thus is only generated in the combustion zone. Hence, thermal NO is ineffective below 1800 K (specifically at z = 60 mm and 80 mm) but instead, NNH mechanism plays a major role in the NO production. Surprisingly, the effect of high H radical produced by SG1 at z=80 mm is less pronounced for production of NO compared to other syngases as shown in Figure 12. This condition is correlated with the stretch rate of flame. Liang et al. [50] reported that flame speed of H_2 increases with stretch rate at rich condition. The increase of stretch rate also reduces the NO production by NNH mechanism as reported by Xie et al. [49]. The high H_2 concentration in SG1 results in high flame speed and the increase of stretch rate in rich mixture proportionally reduces NO from NNH route [49, 51].

The result shows that the composition of SG1 (high H_2-rich syngas) typically produces lower NO and NO_2 species as compared to other types of syngases. The result is consistent with the experimental data in which syngas with high H_2 concentration exhibits lower formation of NO_x, particularly for combustion under premixed mode [52].

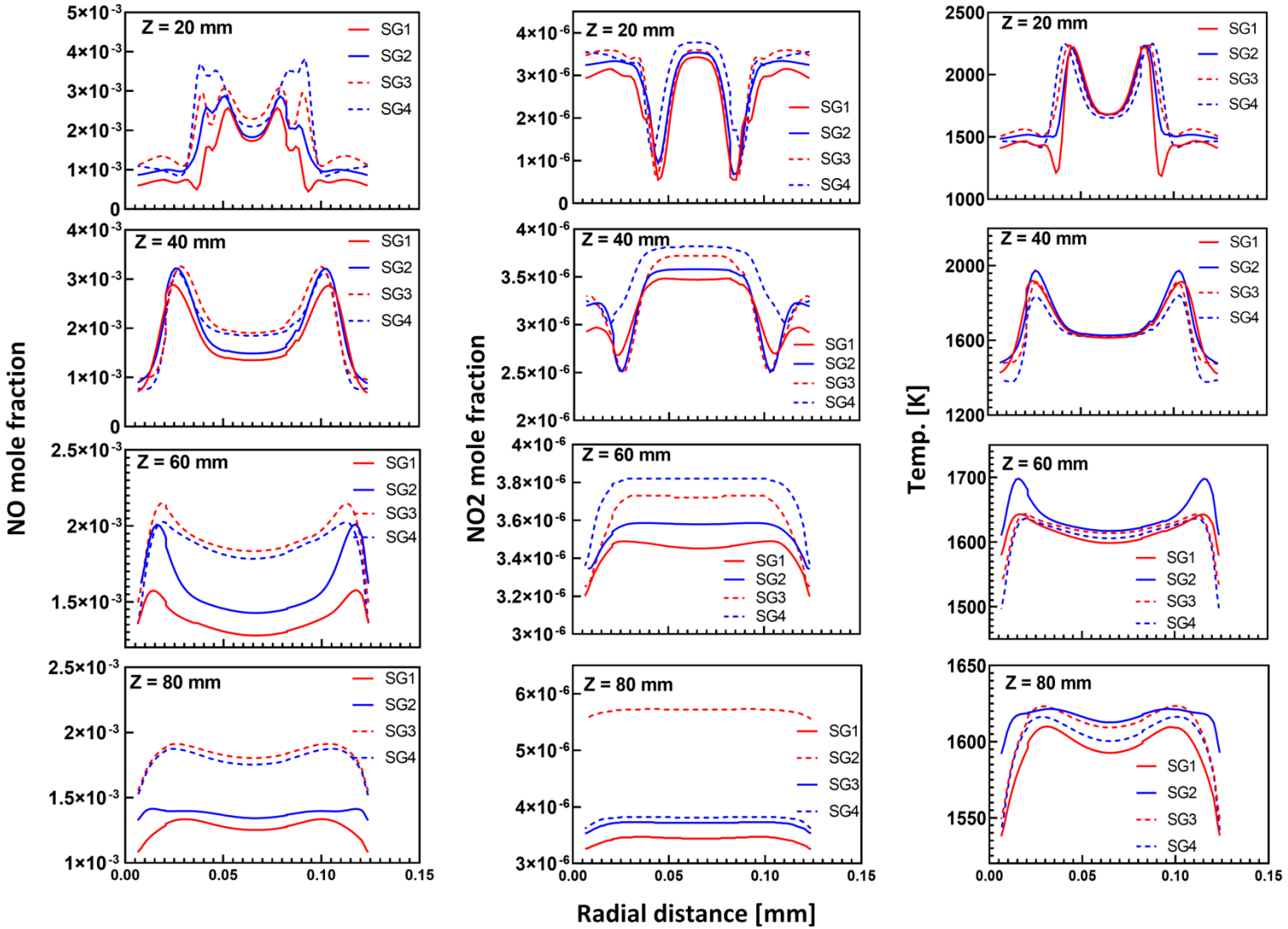

Figure 11: Species of NO, NO_2 and local temperature at reaction zone for different type of syngases

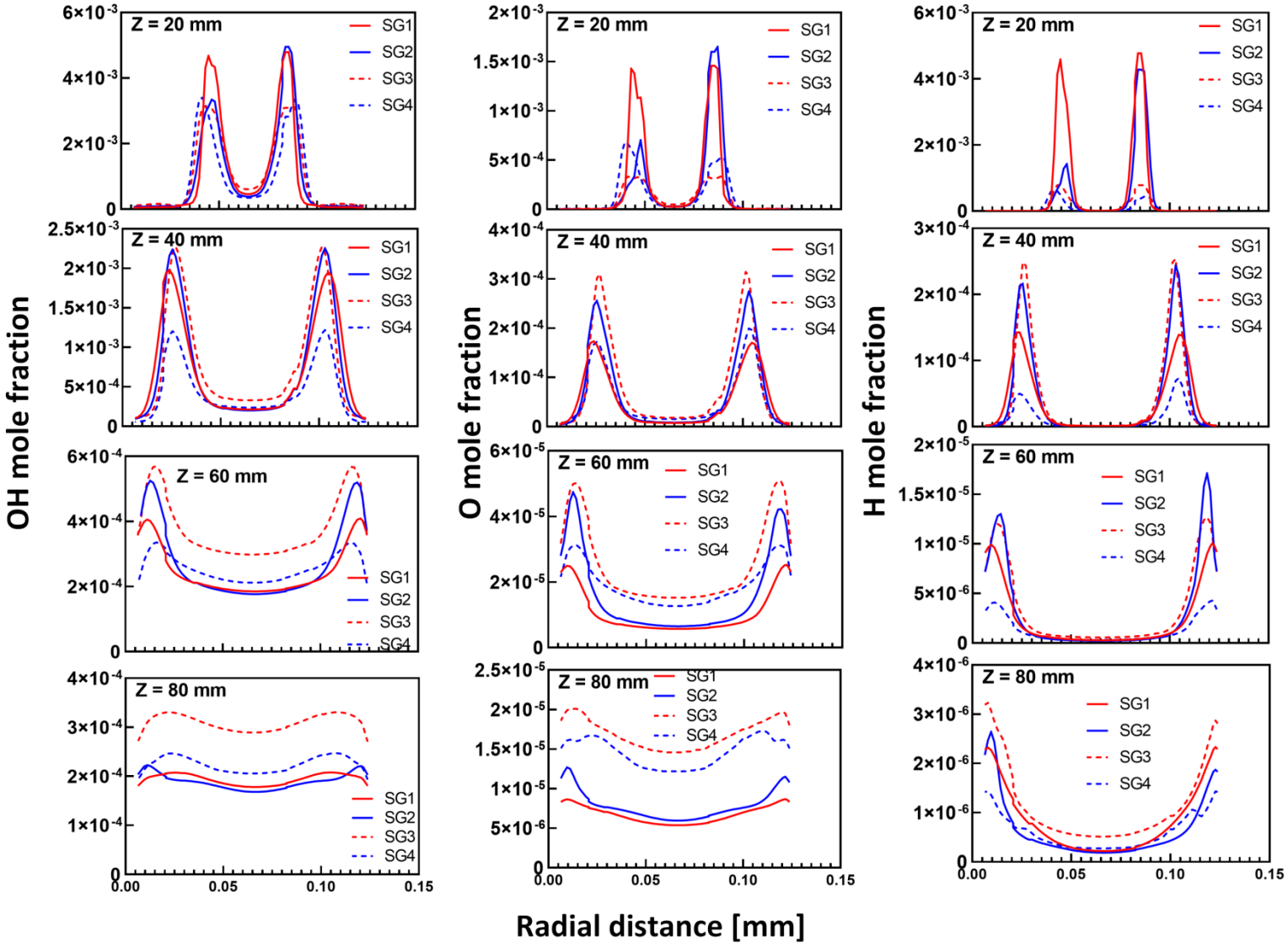

Figure 12: Species distribution of OH, O and H at the reaction zone for different type of syngases

5. Conclusion

The experimental and numerical investigations were conducted to study the flame structure and reactions of syngases in a premixed swirl combustion mode. Validation of the computational work using FGM method with experimental data was performed via the exhaust emission cases. Result shows that FGM method predicts well for CO_2 and O_2 emissions. For NOx emissions, the FGM method agrees well with experimental result at lean condition but over-predicts at stoichiometric region. The temperature distribution within the flame is simulated using FGM method for syngases with different concentration of H_2. High H_2-rich syngas exhibits lower peak temperature, whereas syngas with low concentration of H_2 and high CO produced the highest flame temperature and longest flame. The NO in the reaction zone corresponds to the distribution of local temperature and radical species for all syngas types, notably low flame temperature results in low production of NO species. Hydrogen-enriched syngas exhibits comparatively low NO species in the reaction zone under premixed swirl combustion mode.

Acknowledgement

The funding support from The Royal Society, Malaysian Industry-Government Group for High Technology and The Academy of Sciences Malaysia under the Newton-Ungku Omar Fund: Advanced Fellowship (NA160115) for C.T Chong, Malaysian Ministry of Education and Universiti Teknologi Malaysia (Research University Grant - Tier 1: 17H70) is gratefully acknowledged.

References

[1] García-Armingol T and Ballester J. Operational issues in premixed combustion of hydrogen-enriched and syngas fuels. Int. J. Hydrogen Energy 2015; 40(2): 1229-43.

[2] Samiran NA, Jaafar MNM, Jo-Han Ng, Lam SS, and Chong CT. Progress in biomass gasification technique – With focus on Malaysian palm biomass for syngas production. Renewable Sustainable Energy Rev. 2016; 62: 1047-62.

[3] Chen G, Yao J, Liu J, Yan B, and Shan R. Biomass to hydrogen-rich syngas via catalytic steam reforming of bio-oil. Renewable Energy 2016; 91: 315-22.

[4] Sahoo BB, Sahoo N, and Saha UK. Effect of H2:CO ratio in syngas on the performance of a dual fuel diesel engine operation. Appl. Therm. Eng. 2012; 49: 139-46.

[5] Mansfield AB and Wooldridge MS. The effect of impurities on syngas combustion. Combust. Flame 2015; 162(5): 2286-95.

[6] Caro S, Torres D, and Toledo M. Syngas production from residual biomass of forestry and cereal plantations using hybrid filtration combustion. Int. J. Hydrogen Energy 2015; 40(6): 2568-77.

[7] Hosseini V and Checkel MD. Using Reformer Gas to Enhance HCCI Combustion of CNG in a CFR Engine. 2006; 1.

[8] Azimov U, Tomita E, Kawahara N, and Harada Y. Effect of syngas composition on combustion and exhaust emission characteristics in a pilot-ignited dual-fuel engine operated in PREMIER combustion mode. Int. J. Hydrogen Energy 2011; 36(18): 11985-96.

[9] Safer K, Tabet F, Ouadha A, Safer M, and Gökalp I. Combustion characteristics of hydrogen-rich alternative fuels in counter-flow diffusion flame configuration. Energy Convers. Manage. 2013; 74: 269-78.

[10] Hagos FY, Aziz ARA, and Sulaiman SA. Methane enrichment of syngas (H2/CO) in a spark-ignition directinjection engine: Combustion, performance and emissions comparison with syngas and Compressed Natural Gas. Energy 2015; 90 2006 - 15.

[11] Joo S, Yoon J, Kim J, Lee M, and Yoon Y. NOx emissions characteristics of the partially premixed combustion of H2/CO/CH4 syngas using artificial neural networks. Appl. Therm. Eng. 2015; 80: 436 - 44.

[12] Zhang Y, Zhang H, Tian L, Ji P, and Ma S. Temperature and emissions characteristics of a micro-mixing injection hydrogen-rich syngas flame diluted with N2. Int. J. Hydrogen Energy 2015; 40(36): 12550-59.

[13] Chong CT, Jo-Han N, Aris MS, Mong GR, Shahril NS, Ting ST, and Zulkifli MF. Impact of gas composition variations on flame blowout and spectroscopic characteristics of lean premixed swirl flames. Process Safety and Environmental Protection 2019; 128: 1-13.

[14] Mansouri Z, Aouissi M, and Boushaki T. Numerical computations of premixed propane flame in a swirl-stabilized burner: Effects of hydrogen enrichment, swirl number and equivalence ratio on flame characteristics. Int. J. Hydrogen Energy 2016; 41(22): 9664-78.

[15] Tunçer O, Kaynaroğlu B, Karakaya MC, Kahraman S, Çetiner-Yıldırım O, and Baytaş C. Preliminary investigation of a swirl stabilized premixed combustor. Fuel 2014; 115: 870-74.

[16] De A and Acharya S. Parametric study of upstream flame propagation in hydrogen-enriched premixed combustion: Effects of swirl, geometry and premixedness. Int. J. Hydrogen Energy 2012; 37(19): 14649-68.

[17] Ge B, Tian Y, and Zang S. The effects of humidity on combustion characteristics of a nonpremixed syngas flame. Int. J. Hydrogen Energy 2016; 41(21): 9219-26.

[18] Zhang Y, Shen W, Zhang H, Wu Y, and Lu J. Effects of inert dilution on the propagation and extinction of lean premixed syngas/air flames. Fuel 2015; 157: 115-21.

[19] Alavandi S. Experimental study of combustion of hydrogen–syngas/methane fuel mixtures in a porous burner. Int. J. Hydrogen Energy 2008; 33(4): 1407-15.

[20] Li S, Li S, Mira D, Zhu M, and Jiang X. Investigation of dilution effects on partially premixed swirling syngas flames using a LES-LEM approach. J. Energy Inst. 2017.

[21] Ilbas M and Karyeyen S. Turbulent diffusion flames of a low-calorific value syngas under varying turbulator angles. Energy 2017; 138: 383-93.

[22] Mukhopadhyay S, Bastiaans RJM, Oijen JAv, and Goey LPHd. Analysis of a filtered flamelet approach for coarse DNS of premixed turbulent combustion. Fuel 2015; 144: 388–99.

[23] Nakod P, Yadav R, Rajeshirke P, and Orsino S. A Comparative Computational Fluid Dynamics Study on Flamelet-Generated Manifold and Steady Laminar Flamelet Modeling for Turbulent Flames. J. Eng. Gas Turbines Power 2014; 136(8): 081504.

[24] Verhoeven LM, Ramaekers WJS, van Oijen JA, and de Goey LPH. Modeling non-premixed laminar co-flow flames using flamelet-generated manifolds. Combust. Flame 2012; 159(1): 230-41.

[25] Chong CT, Chiong M-C, Jo-Han Ng, Lim M, Tran M-V, Valera-Medina A, and Chong WWF. Oxygenated sunflower biodiesel: Spectroscopic and emissions quantification under reacting swirl spray conditions. Energy 2019; 178: 804-13.

[26] Tao H-G, Chen H-X, Xie J-L, and Hu Y-P. An alternative approach to quantifying fluid flow uniformity based on area-weighted average velocity and mass-weighted average velocity. Energy Build. 2012; 45: 116-23.

[27] D'Orazio A, Rapagnà S, Foscolo PU, Gallucci K, Nacken M, Heidenreich S, Di Carlo A, and Dell'Era A. Gas conditioning in H2 rich syngas production by biomass steam gasification: Experimental comparison between three innovative ceramic filter candles. Int. J. Hydrogen Energy 2015; 40(23): 7282-90.

[28] Wang K, Yu Q, Qin Q, Hou L, and Duan W. Thermodynamic analysis of syngas generation from biomass using chemical looping gasification method. Int. J. Hydrogen Energy 2016; 41(24): 10346-53.

[29] (2013). ANSYS Fluent Theory Guide.

[30] Turkeli-Ramadan Z, Sharma RN, and Raine RR. Two-dimensional simulation of premixed laminar flame at microscale. Chem. Eng. Sci. 2015; 138: 414-31.

[31] Krieger GC, Campos APV, Takehara MDB, Cunha FAd, and Veras CAG. Numerical simulation of oxy-fuel combustion for gas turbine applications. Appl. Therm. Eng. 2015; 78: 471 - 81.

[32] Mayr B, Prieler R, Demuth M, and Hochenauer C. The usability and limits of the steady flamelet approach in oxy-fuel combustions. Energy 2015; 90: 1478-89.

[33] Mayr B, Prieler R, Demuth M, Potesser M, and Hochenauer C. CFD and experimental analysis of a 115kW natural gas fired lab-scale furnace under oxy-fuel and air–fuel conditions. Fuel 2015; 159: 864-75.

[34] Göktolga MU, van Oijen JA, and de Goey LPH. Modeling MILD combustion using a novel multistage FGM method. Proc. Combust. Inst. 2016.

[35] Ihme M, Shunn L, and Zhang J. Regularization of reaction progress variable for application to flamelet-based combustion models. J. Comput. Phys. 2012; 231(23): 7715-21.

[36] Oijen JAv and Goey LPHd, Predicting NO Formation with Flamelet Generated Manifolds, in *Proceedings of the European Combustion Meeting 2009*. 2009.

[37] Boucher A and Bertier N. A method to extend flamelet manifolds for prediction of NOx and long time scale species with tabulated chemistry. Int. J. Sustainable Aviation 2014; 1(2): 181-202.

[38] Najafi-Yazdi A, Cuenot B, and Mongeau L. Systematic definition of progress variables and Intrinsically Low-Dimensional, Flamelet Generated Manifolds for chemistry tabulation. Combust. Flame 2012; 159(3): 1197-204.

[39] Singh G, Chander S, and Ray A. Heat transfer characteristics of natural gas/air swirling flame impinging on a flat surface. Exp. Therm Fluid Sci. 2012; 41: 165-76.

[40] Oh J, Noh D, and Lee E. The effect of CO addition on the flame behavior of a non-premixed oxy-methane jet in a lab-scale furnace. Applied Energy 2013; 112: 350-57.

[41] Khaleghi M, Hosseini SE, and Abdul Wahid M. Investigations of asymmetric non-premixed meso-scale vortex combustion. Appl. Therm. Eng. 2015; 81: 140-53.

[42] Natarajan J and Seitzman JM. Laminar Flame Properties of H2/CO Mixtures. in: Lieuwen T, Yang V, and Yetter R, Editors.*Synthesis Gas Combustion Fundamentals and Applications*;2010.

[43] Edacheri Veetil J, Rajith CV, and Velamati RK. Numerical simulations of steady perforated-plate stabilized Syngas air pre-mixed flames. Int. J. Hydrogen Energy 2016; 41(31): 13747-57.

[44] Samiran NA, Jo-Han Ng, Mohd Jaafar MN, Valera-Medina A, and Chong CT. Swirl stability and emission characteristics of CO-enriched syngas/air flame in a premixed swirl burner. Process Safety and Environmental Protection 2017.

[45] He D and Yan W. Influences of different diluents on NO emission characteristics of syngas opposed-flow flame. Int. J. Hydrogen Energy 2018.

[46] Williams TC, Shaddix* CR, and Schefer RW. Effect of Syngas Composition and CO2-Diluted Oxygen on Performance of a Premixed Swirl-Stabilized Combustor. Combust. Sci. Technol. 2007; 180(1): 64-88.

[47] Park S and Kim Y. Numerical modeling for structure and NO x formation characteristics of oxygen-enriched syngas turbulent non-premixed jet flames. Int. J. Hydrogen Energy 2017; 42(32): 20809-23.

[48] Sahu AB and Ravikrishna RV. Quantitative LIF measurements and kinetics assessment of NO formation in H 2 /CO syngas–air counterflow diffusion flames. Combust. Flame 2016; 173: 208-28.

[49] Xie T and Wang P, Analysis of NO formation in counter-flow premixed hydrogen-air flame, in *Transactions of the Canadian Society for Mechanical Engineering*. 2013. p. 851-59.

[50] Liang W, Wu F, and Law CK. Extrapolation of laminar flame speeds from stretched flames: Role of finite flame thickness. Proc. Combust. Inst. 2017; 36(1): 1137-43.

[51] Cicoria D and Chan CK. Effects of turbulence and strain rate on hydrogen-enriched high Karlovitz number lean premixed methane flames. Fuel 2018; 211: 754-66.

[52] Samiran NA, Jo-Han Ng, Jaafar MNM, Valera-Medina A, and Chong CT. H2-rich syngas strategy to reduce NOx and CO emissions and improve stability limits under premixed swirl combustion mode. Int. J. Hydrogen Energy 2016; 41(42): 19243-55.